Received: March 21, 2024. Revised: April 20, 2024.

INASS

International Journal of
Intelligent Engineering & Systems

http://www.inass.org/

Improved Fibonacci Search Algorithm for Optimal Power Tracking in DFIG-Based Wind Turbine Systems

Saad M. Alwash[1]* **Osama Qasim Jumah Al-Thahab[1]** **Shamam F. Alwash[1]**

[1]*Department of Electrical Engineering, University of Babylon, Babylon 51002, Iraq*
* Corresponding author's Email: saad.mahdi@uobabylon.edu.iq

Abstract: The paper presents an algorithm for harvesting optimal power points (OPP) utilizing the direct power control (DPC) technique of the dual-fed induction generator (DFIG) wind turbine. The conventional Fibonacci search algorithm (FSA) technique cannot find the exact global peak (GP) strategy and may fail. It proposes a new modified Fibonacci search algorithm (MFSA) to extract (OPP) with variable-speed wind energy turbines (VSWET), which is very important for many people and companies. Among the other different algorithms, the MFSA is more efficient and has a simple strategy to track the optimal power point that depends on calculating the effective speed of the Ω_m in an interval [a, b]. The research paper suggests modifying the Fibonacci-based search on the rotor side conversion (RSC) of a 7.5 KW DFIG in the WECS wind energy conversion strategy. The simulation uses the built-in MATLAB/SIMULINK (R2023a) software. It demonstrates the ease of implementation, lower total harmonic distortion THD and efficiency since it uses a step size that is not fixed based on the Fibonacci sequence.

Keywords: DFIG, DPC, FSA, OPP, GP, B2B converter.

1. Introduction

Renewable energy generation using wind turbine energy, photovoltaic (PV) cells, and fuel cells is an essential technology to minimize global warming and environmental crises. These methods are gaining popularity as the costs of conventional fossil fuels rise and the need to reduce carbon dioxide emissions becomes more urgent. As a result, the world is becoming more aware of the pollution caused by burning non-renewable energy sources. Besides being green energy, the availability of sources and the well-established technology have made power generation using renewable energy more desirable for the energy needs of many parts of the world. For this reason, wind energy is one of the most viable renewable energies for electricity in today's world. So far, World Wind Energy Association (WWEA) global statistics show that 840.9 GW of the total wind energy capacity was installed worldwide at the end of 2022 [1].

According to the criteria for rotor speed control, there are two primary kinds of wind turbine systems: fixed-speed (FSWTs) and modern variable-speed (VSWTs). Thus, permanent magnet synchronous generators (PMSG) and DFIG are the most popular types used in VSWTs [2]. The DFIG is commonly used in high-rated power applications of wind energy turbines due to their stability, high efficiency, powers (active and reactive) that can be controlled separately, low-cost power converter, power factor correction that can be adjusted as desired, and low power loss. To optimize and maximize the power conversion of wind energy into electricity, many algorithms and control methods have recently been presented for the DFIG wind energy turbine system.

In recent decades, many research publications have examined various techniques and algorithms that contribute to capturing the maximum power of VSWTs at different wind speeds. These methods are classified according to measured power: direct power control (DPC), indirect power control (IPC), intelligent algorithms, and modern mixtures to extract the maximum power MPP in WTs [3]. It is categorized into four major control strategies [4]. Among them, the tip-speed ratio TSR control used to

capture the MPPT regulates the speed of the rotor and keeps TSR at its optimum value at different speeds [5]. This approach needs accurate knowledge of the parameters of the wind turbines. The drawback of this method is the cost and initial investment costs of wind speed (conventional or ultrasonic) sensors increase. It also, when the rotor suddenly has rapid variations, causes imprecise wind speed sensors, resulting in deviation when extracting the maximum power. The second method, P&O, is easy and inexpensive, requiring no knowledge of generator parameters or wind speed [6]. The P&O search algorithm for MPPT control is widely utilized in PV energy systems. The drawback of this approach is that larger step sizes result in oscillation around the MPP, whilst smaller step sizes create a slower response and longer convergence time. However, this method has not been proper for tracking the performance of large turbines due to the inertia of wind turbines. This method is only appropriate for small wind turbines. Also, sudden wind fluctuations may cause the wind turbine to operate in an unstable mode. The third technique, power signal feedback (PSF), depends on the peak power curve for wind turbines. Consequently, it is typically necessary to make off-line experimental measurements of the power versus mechanical speed characteristic. The drawback of PSF is that for large-sized WTs with high inertia at low wind speeds, tracking the MPPT can result in oscillation or losing control. The fourth method, known as optimum torque control (OTC), involves adjusting the optimal value of DFIG torque with varying wind speeds. This method offers higher efficiency, simplicity, and good tracking speed. However, it has drawbacks such as dependence on environmental conditions and the need to understand the wind turbine's specifications [7]. Various hybrid solutions for extracting maximum energy from WECS exist to overcome the disadvantages of traditional methods [8]. Several hybrid algorithms use advanced algorithms such as neural networks (NN) and fuzzy logic control (FLC) to maximize the extracted power of WECS [9].

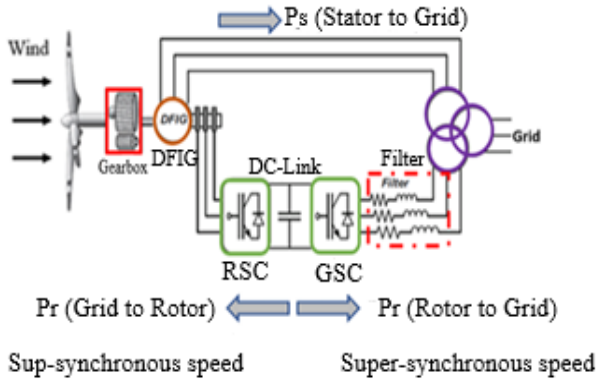

Figure. 1 A typical structure for a DFIG wind generator

The primary objective of this research is modeling DFIG and modifying the FSA algorithm, which is used to control the extraction of OPP. Furthermore, it uses two control strategies: traditional control by proportional-integral (PI) and the proposed new algorithm (FSA). This algorithm has the benefits of reliability, rapid response, minimal computation, and efficiency by utilizing a variable step size based on the Fibonacci sequence.

2. Modelling of WT conversion

The wound rotor, known as a slip-ring asynchronous machine, is fed with supplied AC power from the stator and rotor sides; so, this configuration is called a dual-fed induction machine (DFIM). The three-phase stator windings are directly linked to an infinite electrical network via a transformer. On the other hand, the rotor windings are supplied with a controllable frequency and magnitude voltage by adjusting the B2B converter's modulation index. The three slip-rings are connected to the network via 2PWM back-to-back converters called rotor-side (RSC) and grid-side (GSC), connected by a DC-bus capacitor. Typically, if the generator runs at less than synchronous speed (hypo-speed), the real power flows from the network to the rotor side; the RSC works as DC/AC inverter, and the GSC works as AC/DC rectifier, but if the generator speed runs faster than synchronous speed (hyper-speed), the RSC works as AC/DC rectifier while the GSC works as DC/AC inverter [1]. Fig. 1 depicts a typical (DFIG) wind turbine configuration.

2.1 Aerodynamic mathematical model for WT

The wind turbine converts the aerodynamic energy into mechanical power. The mechanical power extracted by wind turbines is described as follows [7]:

$$P_m = C_p P_{air} = \frac{1}{2}\rho_{air}\pi R^2 v_w^3\, C_p(\lambda,\beta) \quad (1)$$

The power coefficient $C_p(\lambda,\beta)$ is a function of (λ) the tip speed ratio and (β) the blade pitch angle; the wind flow velocity v_w can be written:

$$v_w = \frac{speed\ of\ a\ blad\ tip}{Tip\ speed} = \frac{R\Omega_m}{\lambda} \quad (2)$$

The power expression can be obtained by inserting Eq. (2) into Eq. (1), which can be written as:

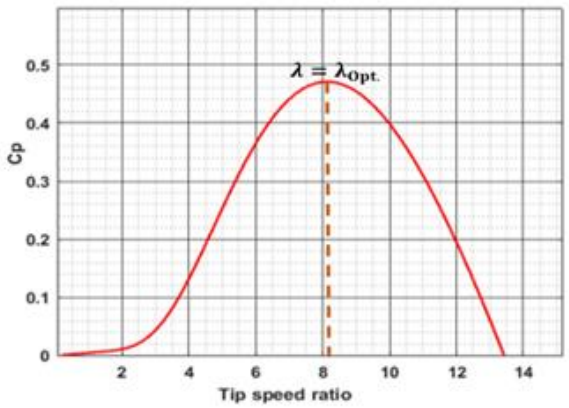

Figure. 2 A typical wind turbine characteristic when fixed-pitch turbine (β ≡ 0)

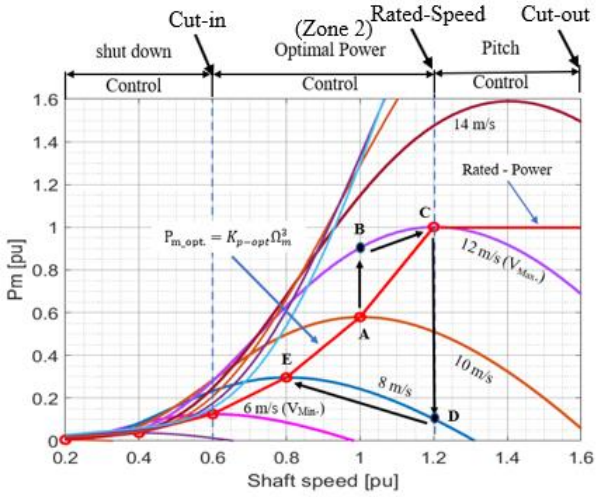

Figure. 3 The power point tracking curve scheme of the typical DFIG

$$P_m = \frac{1}{2\,\lambda^3}\rho_{air}\pi R^5\Omega_m^3\ C_p(\lambda,\beta) \quad (3)$$

One approximate formulation frequently used and easily adapted to the power coefficient estimates for different VSWTs can be described as follows [10]:

$$C_p(\lambda,\beta) = a_1(\frac{a_2}{\lambda_i} - a_3\beta - a_4)(e^{(\frac{a_5}{\lambda_i})}) + a_6\lambda \quad (4)$$

$$\frac{1}{\lambda_i} = \frac{1}{\lambda+0.08\beta} - \frac{0.0035}{\beta^3+1} \quad (5)$$

The values of an approximate coefficients (a_1 *to parameter* a_6): are ($a_1 = 0.5,\ a_2 = 119,\ a_3 = 0.4,\ a_4 = 5,\ a_5 = -21,\ a_6 = 0.0098$). The typical function between the power coefficient and tip-speed ratio is a nonlinear curve for the different values. The pitch angle below the rated wind speed level is set to zero (β=0º) for the MPPT zone, as shown in Fig. 2. Their curve information includes the optimal value tip-speed ratio ($\lambda_{opt.} = 8.1$) and maximum rotor power coefficient $C_{p(opt.)} = 0.48$. Because it is difficult to obtain precise v_w, Eq. (6) usually controls the Ω_m to maximize the power [11, 12].

$$P_{m-pot.}(\Omega_m) = K_{p-opt.}\Omega_m^3 \quad (6)$$

Where:

$$K_{m-opt.} = \frac{1}{2\,\lambda^3}\rho_{air}\pi R^5\ C_p(max.) \quad (7)$$

Fig. 3 depicts the designed wind power system's mechanical power vs rotational speed. The wind turbine can be controlled in three zones, depending on the wind speed: shut-down control, optimal control, and pitch control. Simulation results at the operating zone (2) for optimal power control show that with different wind speeds between cut-in (6 m/s) and the rated (12 m/s), the blade angle (β) control (deactivated) is adjusted to zero degrees. Because it runs in the sub-rated speed range, the mechanical power curve maintains a cubic relationship with the wind speed.

Fig. 3 shows point (A) as the initial optimum operating point with a wind speed $v_w = 10\ m/s$. The wind speed suddenly steps up to $v_w = 12\ m/s$, so the trajectory is from point (A) to point (C), and power from P_A to P_C, which increases the output power. Later, while the system is operated under the clarified parametric uncertainties, the wind speed is suddenly stepped down to $v_w = 8\ m/s$, and the trajectories of the optimum point will be trajected from (C) to (E), and the output power decreases from P_C to P_E. It clarifies that maximum energy output depends not only on the available wind power but also on the operating point at which the energy conversion devices operate.

2.2 Mathematical modelling of the DFIG

In a rotating frame d-axis and q-axis reference, the dynamic voltage vector of the stator and rotor utilizing Park's transformations (abc/dq), DFIG is expressed as follows [13]:

$$v_{qs} = R_s i_{qs} + \frac{d\psi_{qs}}{dt} + \omega_s\psi_{ds} \quad (8)$$

$$v_{ds} = R_s i_{ds} + \frac{d\psi_{ds}}{dt} - \omega_s\psi_{qs} \quad (9)$$

$$v_{dr} = R_r i_{dr} + \frac{d\psi_{dr}}{dt} - \omega_r\psi_{qr} \quad (10)$$

$$v_{qr} = R_r i_{qr} + \frac{d\psi_{qr}}{dt} + \omega_r \psi_{dr} \quad (11)$$

Where:

$$\omega_r = \omega_s - P_p \Omega_m \quad (12)$$

In the reference d-q frame, the flux ψ_s expressions at the stator windings are as follows [14]:

$$\psi_{ds} = L_{ls} i_{ds} + L_m (i_{ds} + i_{dr}) = L_s i_{ds} + L_m i_{dr} \quad (13)$$

$$\psi_{qs} = L_{ls} i_{qs} + L_m (i_{qs} + i_{qr}) = L_s i_{qs} + L_m i_{qr} \quad (14)$$

Also, the flux ψ_r expressions at the rotor windings in the reference d-q frame are:

$$\psi_{qr} = L_{lr} i_{qr} + L_m (i_{qs} + i_{qr}) = L_r i_{qr} + L_m i_{qs} \quad (15)$$

$$\psi_{dr} = L_{lr} i_{dr} + L_m (i_{ds} + i_{dr}) = L_r i_{dr} + L_m i_{ds} \quad (16)$$

Where:

$$L_s = L_{ls} + L_m \quad (17)$$

$$L_r = L_{lr} + L_m \quad (18)$$

When multiplying Eqs. (14) and (15) by L_m and L_s, respectively, the following are obtained:

$$L_m \psi_{qs} = L_m L_s i_{qs} + L_m^2 i_{qr} \quad (19)$$

$$L_s \psi_{qr} = L_s L_r i_{qr} + L_m L_s i_{qs} \quad (20)$$

Eq. (20) is subtracted from Eq. (19), yielding:

$$L_m \psi_{qs} - L_s \psi_{qr} = L_m^2 i_{qr} - L_s L_r i_{qr} \quad (21)$$

Rearrangement Eq. (21):

$$L_s \psi_{qr} = L_m \psi_{qs} + L_s L_r i_{qr} - L_m^2 i_{qr} \quad (22)$$

Now divide Eq. (22) by L_s, and yield.

$$\psi_{qr} = \frac{L_m}{L_s} \psi_{qs} + L_r i_{qr} - \frac{L_m^2}{L_s} i_{qr} \quad (23)$$

$$\psi_{qr} = \frac{L_m}{L_s} \psi_{qs} + L_r \left(1 - \frac{L_m^2}{L_r L_s}\right) i_{qr} \quad (24)$$

$$\psi_{qr} = \frac{L_m}{L_s} \psi_{qs} + \sigma L_r i_{qr} \quad (25)$$

Where the factor σ is the leakage coefficient

$$\sigma = \left(1 - \frac{L_m^2}{L_r L_s}\right) \quad (26)$$

Since $\psi_{qs} = L_m i_m$ and i_m are assumed constants

$$\psi_{qr} = \sigma L_r i_{qr} \quad (27)$$

Similarly,

$$\psi_{dr} = \frac{L_m}{L_s} \psi_{ds} + \sigma L_r i_{dr} \quad (28)$$

The generator's real and reactive powers at the stator and rotor sides of a DFIG can be described using the following equations in a synchronously rotating d/q-axis frame [13]:

$$P_s = \frac{3}{2} (v_{ds} i_{ds} + v_{qs} i_{qs}) \quad (29)$$

$$Q_s = \frac{3}{2} (v_{qs} i_{ds} - v_{ds} i_{qs}) \quad (30)$$

$$P_r = \frac{3}{2} (v_{dr} i_{dr} + v_{qr} i_{qr}) \quad (31)$$

$$Q_r = \frac{3}{2} (v_{qr} i_{dr} - v_{dr} i_{qr}) \quad (32)$$

Analysing the effect of wind on the generator's performance and knowing the performance of DFIG wind turbines require an understanding of the relationship between mechanical and electromagnetic torque [13].

$$T_{em} - T_m = f \Omega_m + J \frac{d\Omega_m}{dt} \quad (33)$$

$$T_{em} = P_p \frac{3 L_m}{2 L_s} (\psi_{ds} i_{qr} - \psi_{qs} i_{dr}) \quad (34)$$

3. RSC and GSC control techniques

The DFIG stator winding are supplied with an infinite electrical three-phase network. Power converters (RSCs) on the rotor side were linked to power converters (GCSs) on the grid side through a DC bus capacitor. According to the MPP curve, RSC current controls the required active and reactive power flow, whereas GSC current regulates DC link voltage and power factor. On the other hand, to achieve various DFIG working conditions, RSC-SVPWM adjusts the rotor current at varying

magnitudes and frequencies according to different mode operations. In order to maximize the transfer of active power from the stator and the rotor circuits to the electrical network, the reactive power references for the RSC and the GSC are typically adjusted to zero. This ensures an approximated power factor equal to one. The flux vector of the stator is aligned with the d-axis, where $\psi_{ds} = \left|\overrightarrow{\psi_s}\right|$ [15].

3.1 GSC current control

The GSC operates by adjusting the output voltage of the B2B-SVPWM converter through a control process. It controls the amplitude and phase of the input d/q current, and subsequently regulates the real and reactive power flowing into the GSC. The GSC and PI aim to regulate the DC-bus voltage by controlling the direct current reference, reducing ripple regardless of rotor power. Since the B2B-GSC converter is not a good choice with a high ripple voltage, its current can heat capacitors over time and cause damage. In fact, the reactive power can be regulated by setting the desired value for the q-axis current reference. The maximum actual power output of the converter can be achieved by operating it in unity PF. This is achieved by fixing the reactive power at zero [15].

The GSC can be modeled by lossless-state reversible switches (DC to AC or AC to DC), and power can be interchanged based on the rotor generator's (hyper, hypo, or synchronous) speed operation. Thus, aligning the grid voltage vector with the active axis $v_{sd}^G = v_s$ of the synchronous frame yields the q-axis component being null ($v_{sq}^G = 0$). As a result, the actual P_g and reactive Q_g power flows between the electrical network and the GSC is given by [16].

$$P_g = \frac{3}{2}\left(v_{sd}^G i_{gd} + v_{sq}^G i_{gq}\right) = \frac{3}{2}\left(v_s i_{gd}\right) \quad (35)$$

$$Q_g = \frac{3}{2}\left(v_{sq}^G i_{gd} - v_{sd}^G i_{gq}\right) = -\frac{3}{2}\left(v_s i_{gq}\right) \quad (36)$$

According to the previous equations, reactive power is proportional to i_{gq}, and active power is proportional to i_{gd}, when the electrical voltage remains constant. According to Fig. 4, the current Equations for the DC-bus capacitor can be written as:

$$C_g \frac{d}{dt} v_{DC} = i_{DC} - i_R \quad (37)$$

When the converter losses are ignored, the following result is obtained:

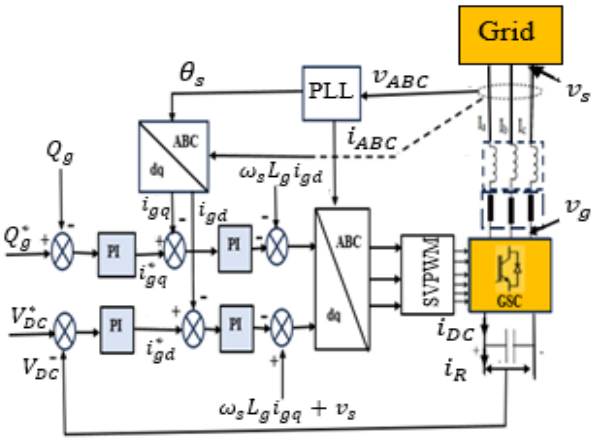

Figure. 4 Diagram of GSC-DFIG control strategy connected to the infinite grid

$$P_g = v_{DC} i_{DC} \quad (38)$$

Substituting Eq. (38) into Eq. (37), getting

$$C_g v_{DC} \frac{d}{dt} v_{DC} + v_{DC} i_R = \frac{3}{2} v_s i_{gd} \quad (39)$$

Eq. (39) shows that i_{gd} can also regulate the converter's DC bus voltage. The d-q voltage equations of the grid-side circuit can be represented as [17]:

$$v_{gd} = R_g i_{gd} + L_g \frac{d}{dt} i_{gd} - \omega_s L_g i_{gq} + v_s \quad (40)$$

$$v_{gq} = R_g i_{gq} + L_g \frac{d}{dt} i_{gq} + \omega_s L_g i_{gd} \quad (41)$$

Using the Clarke transformation of the electrical network voltages, the angular position θ_s is computed as:

$$\theta_s = tan^{-1}\left(\frac{v_{g\beta}}{v_{g\alpha}}\right) \quad (42)$$

3.2 RSC current control

Typically, the RSC technique involves controlling the voltage at the rotor circuit to obtain maximum power point tracking. The rotor voltage Equations for the d/q-axis frame are obtained by substituting Eqs. (27) and (28) into Eqs. (10) and (11) respectively [17].

$$v_{dr} = R_r i_{dr} + \sigma L_r \frac{di_{dr}}{dt} - \omega_r \sigma L_r i_{qr} + \frac{L_m}{L_s} \frac{d\psi_s}{dt} \quad (43)$$

$$v_{qr} = R_r i_{qr} + \sigma L_r \frac{di_{qr}}{dt} + \omega_r \sigma L_r i_{dr} + \omega_r \frac{L_m}{L_s} \psi_s \quad (44)$$

The assumption is that copper losses caused by resistances can be ignored, and the derivative stator flux vector $\frac{d\Psi_s}{dt}$ may be equal to zero because the stator winding supplies an infinite electrical network [18].

$$v_{dr}^{*} = v_{dr} - \omega_r \sigma L_r i_{qr} \quad (45)$$

$$v_{qr}^{*} = v_{qr} + \omega_r \sigma L_r i_{dr} + \omega_r \frac{L_m}{L_s} \psi_s \quad (46)$$

The stator flux vector and the d-axis are aligned in the reference frame $(v_{ds} = 0, v_{qs} = \Psi_s \omega_s = v_s,)$. The power (real/reactive) expression can be derived from Eqs. (29) and (30) (Note that: Ψds=Ψs and Ψqs=0).

$$P_s = \frac{3}{2}\left(\Psi_s \omega_s i_{qs}\right) \quad (47)$$

$$Q_s = \frac{3}{2}(\Psi_s \omega_s i_{ds}) \quad (48)$$

Indeed, the stator current can be expressed as follows using Eqs. (13) and (14):

$$i_{ds} = \frac{\Psi_s - L_m i_{dr}}{L_s} \quad (49)$$

$$i_{qs} = -\frac{L_m i_{qr}}{L_s} \quad (50)$$

Substituting Eq. (50) into Eqs. (47) and (49) into Eq. (48), obtain [13].

$$P_s = -\frac{3}{2}\left(\frac{L_m \Psi_s \omega_s}{L_s} i_{qr}\right) \quad (51)$$

$$Q_s = -\frac{3}{2}\left(\frac{L_m \Psi_s \omega_s}{L_s} i_{dr} - \frac{\Psi_s^2 \omega_s}{L_s}\right) \quad (52)$$

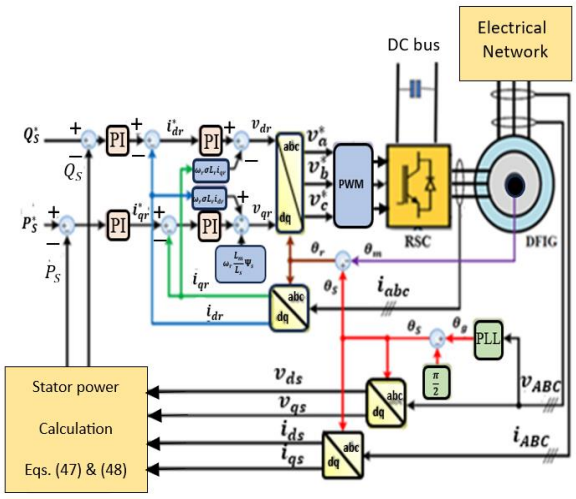

Figure. 5 Diagram of RSC-DFIG control connected to the infinite grid

Eqs. (51) and (52) indicate that the i_{qr} and the i_{dr} current are proportionately related to the stator's P_s and Q_s power respectively [19].

4. Improved fibonacci search algorithm

The modified Fibonacci search algorithm is an accurate one that can find the extracted maximum power and is more efficient since it is not a fixed step size and does not need prior knowledge of all the generator's parameters. Fibonacci numbers are essentially required for the Fibonacci search algorithm. The Fibonacci series F_n is the sum of its previous two numbers. Initial conditions: first and second numbers equal one; the Fibonacci sequence is represented as follows:

$$F_0 = 1, F_1 = 1 \quad (53)$$

$$F_n = F_{n-2} + F_{n-1} \quad \text{for} \quad n \geq 2 \quad (54)$$

Where F_n is the nth generation Fibonacci number, while n denotes the total iterations of experiments to be conducted, the Fibonacci series F_n used in the search algorithm can be described as follows [20].

n	0	1	2	3	4	5	6	7	…..
F_n	1	1	2	3	5	8	13	21	…..

By selecting a suitable search interval [a b] of the MPPT range, “a” is the cut-in point, and “b” is the rated speed point, assuming that initial interval uncertainty $(L_o = b - a)$. Initially, the technique begins with a choice of two possible points Ω_1 and Ω_2, where $\Omega_1 < \Omega_2$ in the specified range for the first two-point experiments [21].

$$\Omega_1 = a + \left(\frac{F_{n-2}}{F_n}\right)(b - a) \quad (55)$$

$$\Omega_2 = b - \left(\frac{F_{n-2}}{F_n}\right)(b - a) \quad (56)$$

Compute the functions $P(\Omega_1)$ and $P(\Omega_2)$. The function's maximum output value is at two checkpoints in the interval range, and then the processing decides whether the direction shifting can be right or left. Fig. 6 depicts the process of limiting and shifting.

There are three cases for the interval of uncertainty, as follows:

Case A: $P(\Omega_1) > P(\Omega_2)$, when the maximum must occur in the interval $[a\ b]$, eliminate the subinterval $[\Omega_2, b]$, then shift the search interval to the left, setting $b^i = \Omega_2$ on the interval $[a, \Omega_2]^i$, the

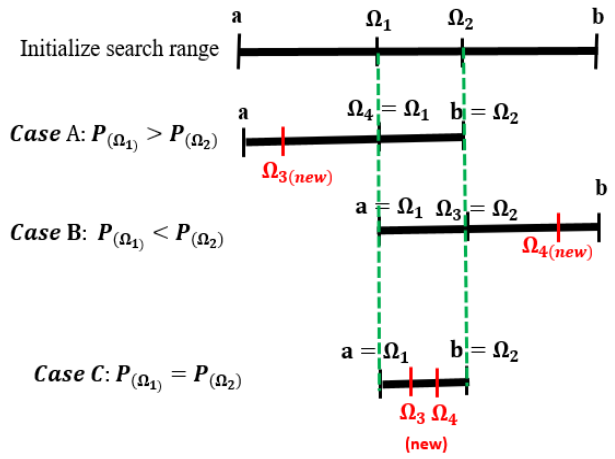

Figure. 6 The shifts in the FSA search process of the MPPT

$\Omega_{1,}^{i}$ and Ω_2^i new test points.

Case B: $P(\Omega_1) < P(\Omega_2)$, when the maximum must occur in the interval $[a\ b]$, eliminate the interval $[a, \Omega_1]$, then shift the search interval to the right, set $a^i = \Omega_1$, the $\Omega_{1,}^{i}$ and Ω_2^i new test points.

Case C: $P(\Omega_1) = P(\Omega_2)$, when the maximum must occur in the interval $[a\ b]$, eliminate the interval $[a, \Omega_1]$ and eliminate the interval $[\Omega_2, b]$, then both Ω_1^i and Ω_2^i as new experimental points.

$$\Omega_{1(new)}^{i} = a^i + \frac{F_{n-j}}{F_{n-j+2}}(b-a)^i \quad (57)$$

$$\Omega_{2(new)}^{i} = b^i - \frac{F_{n-j}}{F_{n-j+2}}(b-a)^i \quad (58)$$

Where j denotes a variable with a beginning value (j=2) in the FSA. Here $\Omega^{(j)}$ and $P_{(\Omega)}^{(j)}$represent shaft speed and mechanical power, respectively [22].

Then, by an iteration process, the initial box of the range must be reduced to a sufficiently small box region, including the peak point of power solution $P(\Omega_j)$ for the interval in which the maximum (power versus shaft speed) lies. This narrowing can be achieved by knowing the function values at two locations within the range. If the optimal power point is to be out of the search range due to a sudden change in wind speed, the search range should continue to shift in the right or left direction curve according to the result algorithm value of maximum power. The search is completed at the n sub-interval, providing that $\left|P_{(\Omega 1)}^{(j)} - P_{(\Omega 2)}^{(j)}\right| \leq \delta$ where δ is the user-specified tolerance and$|L_n/L_o| = \varepsilon$ where ε is the ratio that allows to reach the desired accuracy in locating the optimal power during variable wind speed and $L_n = |b_n - a_n|$, L_n denotes the interval of uncertainty after n experiments. The search is completed when the conditions are met $\left|P_{(\Omega 1)}^{(j)} - P_{(\Omega 2)}^{(j)}\right| \leq \delta$ and $|L_n/L_o| = \varepsilon$. Generally, the smaller the ratio and the tolerance, the more precise the search [23]. Fig. 7 depicts a complete flow chart of the MFSA-based MPPT.

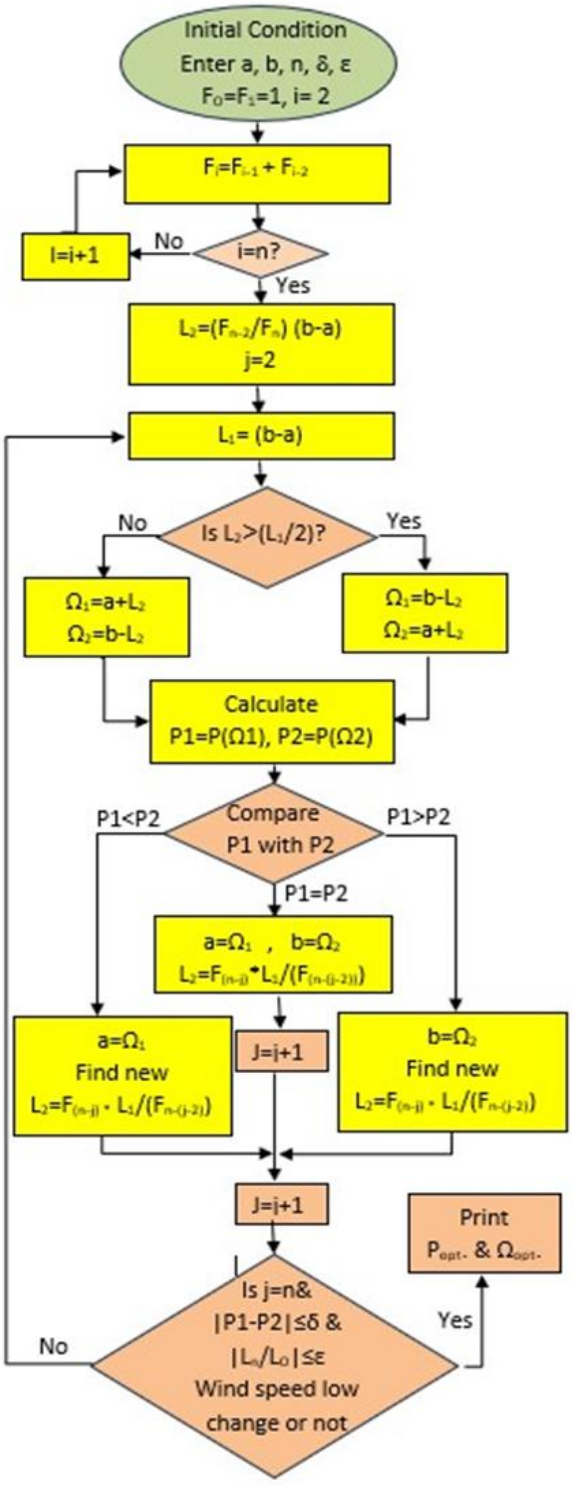

Figure. 7 Depicts a complete flow chart of the MFSA-based MPPT

Proposed search algorithm has been summarized as follows:

Algorithm

Step 1: Initial period of uncertainty by selecting the lower limit “a” and the upper limit "b", in which included the optimum global point between them, compute the “n” which is the no. of iterations according to the “ε” ratio allows, and select the “δ” which is the specified tolerance.

Step 2: Generate the sequence of Fibonacci numbers F_n.

Step 3: Compute initial interval $L_o = b - a$.

Step 4: A comparison is made to ensure that (Ω_1) always lies to the left of (Ω_2).

Step 5: Calculate the power values P_1 and P_2.

Step 6: The value of the (P1&P2) at two checkpoints decides the direction of the tracking; shifting can be either to the left or right.

Step 7: Set the new search interval, generate new search points and calculate the corresponding power.

Step 8: Steps 4 to 7 must be repeated until the optimal peak is found with the necessary accuracy.

Step 9: If wind speed changes, go to Step 3; otherwise, evaluate maximal power $P_m = Max.(P_1 P_2 \dots P_n)$.

The simulation Fibonacci search algorithm is implemented using the built-in function block in MATLAB/SIMULINK. The embedded function block gives the reference power, which is then compared to the actual power at which the wind turbine operates. The error signal will be fed to the PI-type regulator block, and the output signal is then fed a modulation technique SVPWM to generate an accurate pulse to drive the back-to-back converters [17, 24, 25].

5. Results and discussion

A 7.5-KW DFIG-based converter for wind energy was designed and simulated in MATLAB SIMULINK using conventional vector control (DPC) and MFSA control, as depicted in Fig. 8. The study uses a simulation time of 1.4 seconds. Fig. 3 displays the various curves for wind speeds ranging from (6 m/s to 12 m/s). The shaft speed of a DFIG in MPPT control varies from about (0.6-1.2) pu.

Fig. 9 displays the functioning of a DFIG when it operates at synchronous speed. Indeed, it operates in both (hypo and hyper) synchronous modes, as shown in Fig.10.

Fig. 11 illustrates the comparison between the reference (about 0.9-time synchronous speed), and actual speed versus time for the controller system.
The stator current waveform and the THD analysis factor corresponding to the stator current from (0 to 1000) Hz, with a fundamental frequency of about 50 Hz are presented in Figs. 12 and 13, respectively. This clearly shows that the THD percentage in the stator's current based on MFSA and PI are only 18.07 % and 20.12% respectively when the generator runs at its rated speed. The MFSA algorithms provide better results than others, with less THD and better

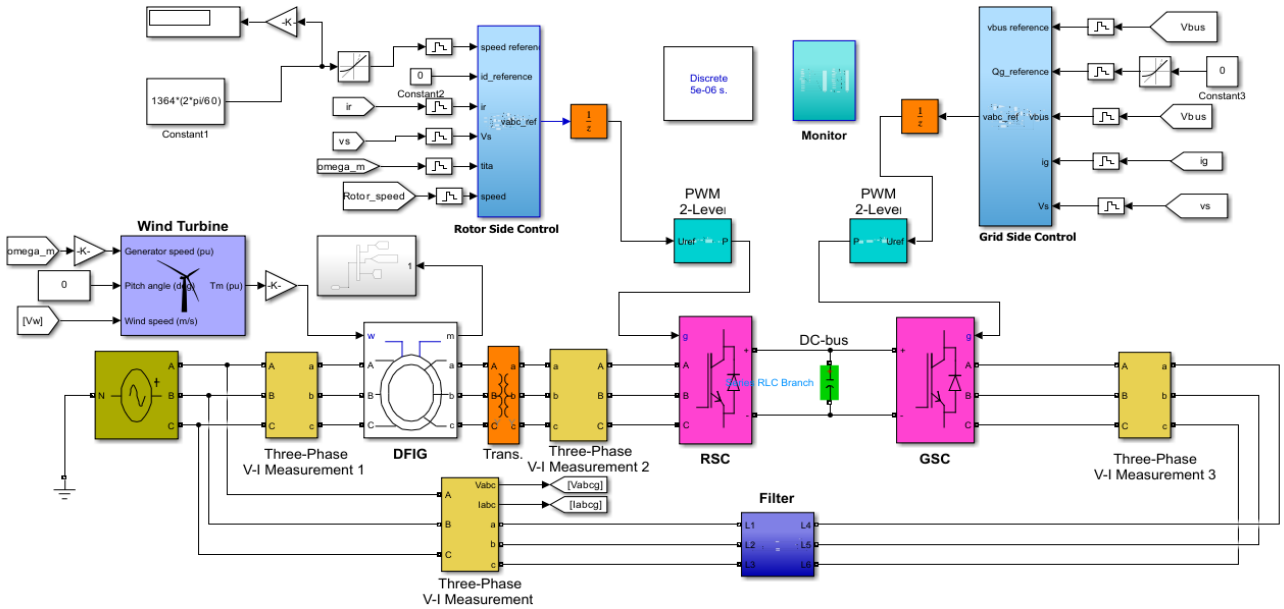

Figure. 8 Complete simulation model for the DFIG-based wind turbine

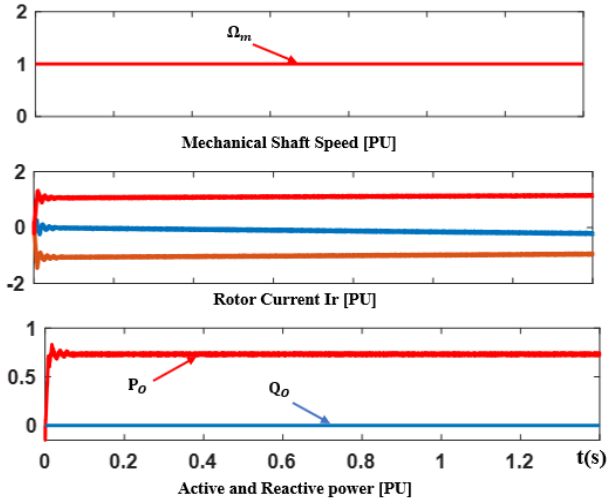

Figure. 9 Typical simulations in WECS at synchronous mode

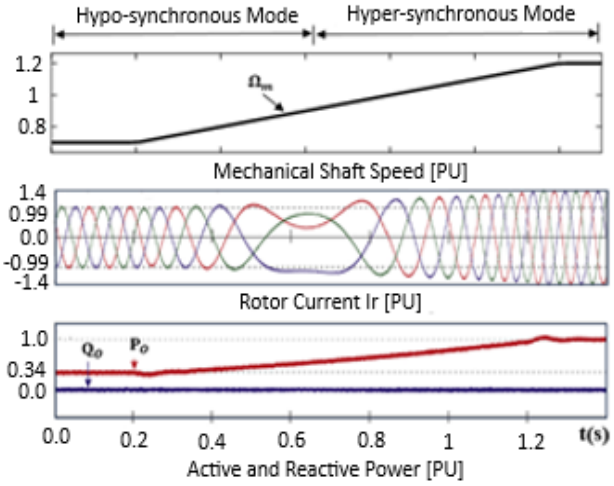

Figure. 10 Typical WECS transitions from hypo-synchronous to hyper-synchronous mode

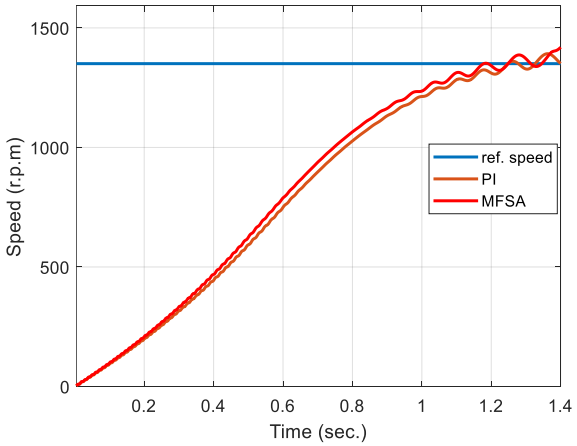

Figure. 11 Comparison between (PI and MFSA) responses with the reference (about 0.9-time synchronous speed)

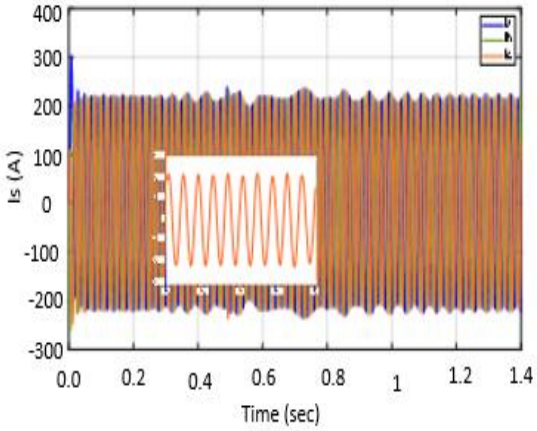

Figure. 12 The stator current's waveform

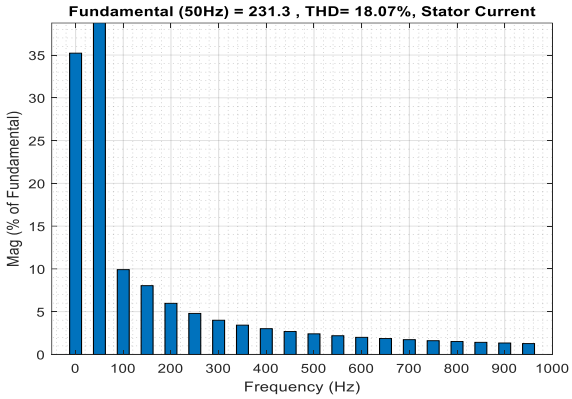

(a)

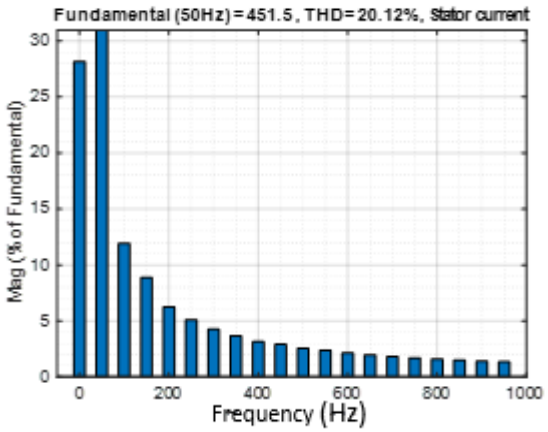

(b)

Figure. 13 The THD harmonic analysis of stator current based on MFSA and PI: (a) MFSA and (b) PI

transient operation.

The actual work compares the performance of two control systems, PI-based and FSA approaches, for DFIG wind turbines operating in an optimal power zone. As can be seen from Figs. 11-13, the suggested control provides a good response because the response is close to its reference, so the error stays bounded at zero. This algorithm has the benefits of

reliability, rapid response, and minimal computation. It shows the simplicity of implementing (MFSA) using microcontrollers or (FPGAs) field programmable gate arrays and efficiency by utilizing a variable step size based on the Fibonacci sequence.

6. Conclusion

In this work, a new algorithm technique that utilizes the Fibonacci line search for the MPPT control in WECS is presented. Moreover, a direct power control approach for DFIG drives controlling the actual and reactive powers is being proposed. The direct power control method employs a novel algorithm based on an enhanced Fibonacci search technique that exhibits fast dynamic response and steady-state performance, making it suitable for power wind energy operations. The simulation results demonstrate the efficient operation of the suggested technique under wind changes with smooth speed tracking, less overshoot, and quick response. The challenge is that a sudden change in wind speed can cause the MPP to get lost in the case of large or medium-sized wind turbines.

In future directions, to eliminate this problem, hybrid methods combining fuzzy logic and a lookup table-based MPPT method with the MFSA have been suggested.

Table 1. Shows the specific characteristics of DFIG, which were utilized as simulation parameters

Parameters	Value (units)
Rated power (P_g) DFIG	7.5 (KW)
Stator winding rated voltage	400 (V)
Total Moment of inertia J	0.15 (Kg.m^2)
Total Friction factor constant	0.05(N.m.s)
No. of P_p	2
Supply frequency	50 (Hz)
R_s	0.5968 (Ω)
R_r	0.6258 (Ω)
L_{is}	0.00547 (H)
L_{ir}	0.00547 (H)
L_m	0.0354 (H)

Table 2. Shows the specific characteristics of wind turbine, which were utilized as simulation parameters

Parameters	Value (units)
Cut-in speed	6 (m/s)
Rated speed	12 (m/s)
Cut-out speed	18 (m/s)
Blade radius (R)	3.18 (m)
Optimal tip-speed ratio ($\lambda_{opt.}$)	8.1
Optimal power coefficient (C_p)	0.48
Blade pitch angle (β)	0

Nomenclature:

DFIG	Dual-fed induction generator
PMSG	Permanent magnet synchronous generators
DPC	Direct power control
IPC	Indirect power control
P&O	Perturb and Observation search algorithm
PF	Power Factor
MPPT	Maximum Power Point Tracking
WECS	Wind Energy Conversion Systems
THD	Total Harmonic Distortion
WT	Wind Turbine
GSC	Grid side converter
RSC	Rotor side converter
FFT	Fast fourier transform
L_m	Mutual inductance, H
L_s, L_r	Stator and rotor self-inductances, H
Rs, R_r	Stator and rotor winding resistances, Ω
Ψ_{ds}, Ψ_{qs}	Stator flux vector in d,q-axis, Wb
Ψ_{dr}, Ψ_{qr}	Rotor flux vector in d,q-axis, Wb
i_{ds}, i_{qs}, i_{dr}, i_{qr}	Stator and rotor current in d,q-axis, A
v_{ds}, v_{qs}	Stator voltage in d,q components, V
v_{dr},v_{qr}	Rotor voltage in d,q components, V
P_s, Q_s	Active and reactive powers of stator, Kw
P_r, Q_r	Active and reactive powers of rotor, Kw
e_{P_s}, e_{Q_S}	Errors active and reactive stator power
Ω_m	Rotational speed of the wind turbine, (rad/sec).
T_{em}	Electromagnetic torque, N·m
T_m	Mechanical torque, N·m
P_p	No. of pole pairs
R	Blade radius, m^2
v_w	Wind speed, m/s
C_p	Power co-efficient
ω_s	Synchronous angular speed, rad/sec
ω_r	Angular speed of rotor, rad/sec
Greek symbols	
ρ_{air}	1.225 kg/m^3 air density in kg/m^3, (e.g., and a temperature of 15°C at sea level).
β	Blade pitch angle
λ	Tip speed ratio
σ	Leakage coeffiecient

Conflicts of Interest

The authors declare no conflict of interest.

Author Contributions

The corresponding author, Saad M. Alwash proposed the structure, wrote the manuscript, and modelled the WECS and the proposed MFSA -DPC method using MATLAB software (R2023a). The supervisors Osama Qasim Jumah Al-Thahab and Shamam F. Alwash, contributed to performing and

revising the manuscript. All authors read and approved the manuscript.

Funding

The research work is not supported by any funding agency.

References

[1] J. Pande, P. Nasikkar, K. Kotecha, and V. Varadarajan, "A review of maximum power point tracking algorithms for wind energy conversion systems", *J Mar Sci Eng*, Vol. 9, No. 11, p. 1187, 2021, doi: 10.3390/jmse9111187.

[2] S. M. Alwash, O. Q. J. Al-Thahab, and S. Alwash, "A Review of Control Techniques Future Trends in Wind Energy Turbine Systems with Doubly Fed Induction Generators (DFIG)", *Journal of University of Babylon for Engineering Sciences*, Vol. 31, No. 7, pp. 32-50, 2023.

[3] J. Wang and D. Bo, "Adaptive fixed-time sensorless maximum power point tracking control scheme for DFIG wind energy conversion system", *International Journal of Electrical Power & Energy Systems*, Vol. 135, p. 107424, 2022, doi: 10.1016/j.ijepes.2021.107424.

[4] M. Abdelateef Mostafa, E. A. El-Hay, and M. M. ELkholy, "Recent trends in wind energy conversion system with grid integration based on soft computing methods: comprehensive review, comparisons and insights", *Archives of Computational Methods in Engineering*, Vol. 30, No.3, pp. 1439-1478, 2023, doi: 10.1007/s11831-022-09842-4.

[5] D. Zouheyr, B. Lotfi, and B. Abdelmadjid, "Improved hardware implementation of a TSR based MPPT algorithm for a low cost connected wind turbine emulator under unbalanced wind speeds", *Energy*, Vol. 232, p. 121039, 2021, doi: 10.1016/j.energy.2021.121039.

[6] I. Toumi, B. Meghni, O. Hachana, A. T. Azar, A. Boulmmaiz, A. J. Humaidi, I. K. Ibraheem, N.A.Kamal, Q.zhu, G.Fusco, and N.K. Bahgaaat, "Robust variable-step perturb-and-observe sliding mode controller for grid-connected wind-energy-conversion systems", *Entropy*, Vol. 24, No. 5, p. 731, 2022, doi: 10.3390/e24050731.

[7] M. Yin, W. Li, C. Y. Chung, L. Zhou, Z. Chen, and Y. Zou, "Optimal torque control based on effective tracking range for maximum power point tracking of wind turbines under varying wind conditions", *IET Renewable power generation*, Vol. 11, No. 4, pp. 501-510, 2017. doi: 10.1049/iet-rpg.2016.0635.

[8] B. Desalegn, D. Gebeyehu, and B. Tamrat, "Wind energy conversion technologies and engineering approaches to enhancing wind power generation: A review", *Heliyon*, Vol. 8, No. 11, 2022, doi: 10.1016/j.heliyon.2022.e11263.

[9] K. Belmokhtar, M. L. Doumbia, and K. Agbossou, "Novel fuzzy logic based sensorless maximum power point tracking strategy for wind turbine systems driven DFIG (doubly-fed induction generator) ", *Energy*, Vol. 76, pp. 679-693, 2014, doi: 10.1016/j.energy.2014.08.066

[10] Y. S. Bouziane, N. Henini, and A. Tlemçani, "Energy Management of a Hybrid Generation System Based on Wind Turbine Coupled with a Battery/Supercapacitor", *Journal Européen des Systèmes Automatisés*, Vol. 55, No. 5, pp. 623-631, 2022, doi: 10.18280/jesa.550507.

[11] L. J. Ontiveros, P. E. Mercado, and G. O. Suvire, "A new model of the double-feed induction generator wind turbine," In: *Proc. Transmission and Distribution Conference and Exposition: Latin America (T&D-LA), IEEE*, pp. 263-269, 2010, doi: 10.1109/TDC-LA.2010.5762892.

[12] D. C. Phan and S. Yamamoto, "Maximum energy output of a DFIG wind turbine using an improved MPPT-curve method", *Energies (Basel*), Vol. 8, No. 10, pp. 11718-11736, 2015, doi: 10.3390/en81011718.

[13] S. M. Alwash, O. Q. J. Al-Thahab, and S. F. Alwash, "Modeling and Control Strategies for DFIG in Wind Turbines: A Comparative Analysis of SPWM, THIPWM, and SVPWM Techniques", *Journal Européen des Systèmes Automatisés*, Vol. 56, No. 6, pp. 963-972, 2023, doi: 10.18280/jesa.560607.

[14] O. E. Elbashir, W. Zezhong, and L. Qihui, "Modeling and analysis of DFIG in wind energy conversion system", *Int. J. Energy Environ*, Vol. 5, No. 2, pp. 239-250, 2014.

[15] F. Guo, T. Zheng, and Z. Wang, "Comparative study of direct power control with vector control for rotor side converter of DFIG", In*: Proc. 9th IET International Conference on Advances in Power System Control, Operation and Management (APSCOM), Hong Kong*, pp. 1-6, 2012, doi: 10.1049/cp.2012.2126.

[16] M. Sleiman, B. Kedjar, A. Hamadi, K. Al-Haddad, and H. Y. Kanaan, "Modeling, control and simulation of DFIG for maximum power point tracking", In: *Proc. 9th Asian Control Conference (ASCC), IEEE, Istanbul, Turkey*, pp. 1-6, 2013, soi: 10.1109/ASCC.2013.6606327.

[17] A. A. Chhipą, P. Chakrabarti, V. Bolshev, T. Chakrabarti, G. Samarin, A. N. Vasilyev, S. Ghosh, and A. Kudryavtsev, "Modeling and

control strategy of wind energy conversion system with grid-connected doubly-fed induction generator", *Energies (Basel)*, Vol. 15, No. 18, p. 6694, 2022, doi: 10.3390/en15186694.

[18] S. Abdi Yonis, Z. Yusupov, A. Habbal, and O. Toirov, "Control Approach of a Grid Connected Dfig Based Wind Turbine Using Mppt and Pi Controller", *Advances in Electrical and Electronic Engineering*, Vol. 21, No. 3, pp. 157-170, 2023.

[19] B. Aljafari, J. Pamela Stephenraj, I. Vairavasundaram, and R. Singh Rassiah, "Steady state modeling and performance analysis of a wind turbine-based doubly fed induction generator system with rotor control", *Energies (Basel)*, Vol. 15, No. 9, p. 3327, 2022, doi: 10.3390/en15093327.

[20] M. Subasi, N. Yildirim, and B. Yildiz, "An improvement on Fibonacci search method in optimization theory", *Appl Math Comput*, Vol. 147, No. 3, pp. 893-901, 2004, doi: 10.1016/S0096-3003(02)00828-7.

[21] S. Malathy and R. Ramaprabha, "Maximum power point tracking algorithm of SPVA under inhomogeneous irradiation conditions: a modified Fibonacci search based approach", In: Proc. *IEEE 12th International Conference on Power Electronics and Drive Systems(PEDS), Honolulu, USA*, pp. 487-492, 2017, doi: 10.1109/PEDS.2017.8289159.

[22] I. Yazici, E. K. Yaylacı, B. Cevher, F. Yalçın, and C. Yüzkollar, "A new MPPT method based on a modified Fibonacci search algorithm for wind energy conversion systems", *Journal of Renewable and Sustainable Energy*, Vol. 13, No. 1, 2021, doi: 10.1063/5.0035134.

[23] J.-H. Zhang, X.-Y. Wei, L. Hu, and J.-G. Ma, "A MPPT method based on improved fibonacci search photovoltaic array", *Tehnički vjesnik*, Vol. 26, No. 1, pp. 163-170, 2019, doi: 10.17559/TV-20180721153103.

[24] A. Pozo, E. Ayala, S. Simani, and E. Muñoz, "Indirect speed control strategy for maximum power point tracking of the DFIG wind turbine system", *Revista Técnica Energía*, Vol. 17, No. 2, pp. 92-101, 2021.

[25] A. Mehdi, A. Reama, H. E. Medouce, S. E. Rezgui, and H. Benalla, "Direct active and reactive power control of DFIG based wind energy conversion system", *International Symposium on Power Electronics, Electrical Drives, Automation and Motion, IEEE*, pp. 1128-1133, 2014, doi: 10.1109/SP EEDAM.2014.6872091.